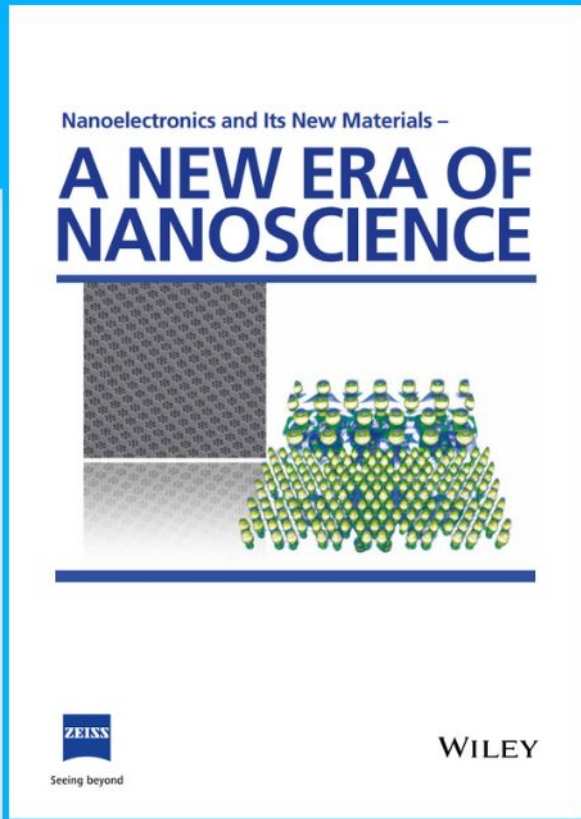




Nanoelectronics and Its New Materials – A NEW ERA OF NANOSCIENCE



Discover the recent advances in electronics research and fundamental nanoscience.

Nanotechnology has become the driving force behind breakthroughs in engineering, materials science, physics, chemistry, and biological sciences. In this compendium, we delve into a wide range of novel applications that highlight recent advances in electronics research and fundamental nanoscience. From surface analysis and defect detection to tailored optical functionality and transparent nanowire electrodes, this eBook covers key topics that will revolutionize the future of electronics.

To get your hands on this valuable resource and unleash the power of nanotechnology, simply download the eBook now. Stay ahead of the curve and embrace the future of electronics with nanoscience as your guide.



Seeing beyond

WILEY

Sphagnum Inspired g-C₃N₄ Nano/Microspheres with Smaller Bandgap in Heterojunction Membranes for Sunlight-Driven Water Purification

Lingtong Ji, Luke Yan, Min Chao,* Mengru Li, Jincui Gu,* Miao Lei, Yanmei Zhang, Xun Wang,* Junyuan Xia, Tianyu Chen, Yujing Nie, and Tao Chen*

Membrane separation is recognized as one of the most effective strategies to treat the complicated wastewater system for economic development. However, serious membrane fouling has restricted its further application. Inspired by sphagnum, a 0D/2D heterojunction composite membrane is engineered by depositing graphitic carbon nitride nano/microspheres (CNMS) with plentiful wrinkles onto the polyacrylic acid functionalized carbon nanotubes (CNTs-PAA) membrane through hydrogen bond force. Through coupling unique structure and chemistry properties, the CNTs-PAA/CNMS heterojunction membrane presents superhydrophilicity and underwater superoleophobicity. Furthermore, thanks to the J-type aggregates during the solvothermal process, it is provided with a smaller bandgap (1.77 eV) than the traditional graphitic carbon nitride (g-C₃N₄) sheets-based membranes (2.4–2.8 eV). This feature endows the CNTs-PAA/CNMS membrane with superior visible-light-driven self-cleaning ability, which can maintain its excellent emulsion separation (with a maximum flux of $5557 \pm 331 \text{ L m}^{-2} \text{ h}^{-1} \text{ bar}^{-1}$ and an efficiency of $98.5 \pm 0.6\%$), photocatalytic degradation (with an efficiency of $99.7 \pm 0.2\%$), and antibacterial (with an efficiency of $\approx 100\%$) ability even after cyclic experimental processes. The excellent self-cleaning performance of this all-in-one membrane represents its potential value for water purification.


treatment technology an extremely tough task.^[1] Currently, membrane separation technology has become the main channel to remediate the water environment attributing to its advantages, such as environmental sustainability and energy saving.^[2] Particularly, graphene oxide (GO) and carbon nanotubes (CNTs), have attracted comprehensive attention on constructing multifunctional separation membranes in the scientific field.^[3] For one thing, they possess high surface areas that are beneficial to achieve effective adsorption with water-soluble pollutants (dye molecules, bacteria, et al.).^[4] For another, they can be taken as secondary reaction platforms for designing functional membranes through chemical crosslinking, interface assembly, and nanoparticle modification, which will enhance their capture ability for target compounds.^[5] To date, the research on carbon-based membranes with versatility has brought inspiring achievements. For example, Liu and co-workers have designed a SiO₂/GO composite membrane through the modification of SiO₂ nanoparticle and ethylenediamine.^[6] It can purify the oil-in-water (O/W) emulsion with the flux of $470 \text{ L m}^{-2} \text{ h}^{-1}$ and high retention capacity for dye molecules. Chen et al. have constructed a series of superhydrophilic CNTs-based composite membranes via hydrophilic

1. Introduction

With thousands of hazardous contaminations, polluted water has become a primary environmental concern in various domains of human society, which searched for generic water

L. T. Ji, Prof. L. K. Yan, Prof. M. Chao, M. R. Li, M. Lei, Y. M. Zhang, Prof. T. Chen
Polymer Materials & Engineering Department
School of Materials Science & Engineering
Chang'an University
Xian 710064, China
E-mail: chaomin@chd.edu.cn; tao.chen@nimte.ac.cn

Dr. J. C. Gu, J. Y. Xia, T. Y. Chen, Prof. T. Chen
Key Laboratory of Marine Materials and Related Technologies
Zhejiang Key Laboratory of Marine Materials and Protective Technologies
Ningbo Institute of Material Technology and Engineering
Chinese Academy of Science
Ningbo 315201, China
E-mail: gujincui@nimte.ac.cn

 The ORCID identification number(s) for the author(s) of this article can be found under <https://doi.org/10.1002/smll.202007122>.

Dr. J. C. Gu, Prof. T. Chen
School of Chemical Sciences
University of Chinese Academy of Science
Beijing 100049, China

Prof. X. Wang
Key Lab of Organic Optoelectronics and Molecular Engineering
Department of Chemistry
Tsinghua University
Beijing 100084, China
E-mail: wangxun@mail.tsinghua.edu.cn

Prof. Y. J. Nie
Fujian Province University Key Laboratory of Modern Analytical Science and Separation Technology
College of Chemistry
Chemical Engineering and Environment
Minnan Normal University
Zhangzhou 363000, China

DOI: 10.1002/smll.202007122

polymer functionalization as well as subsequent assembly of nanoparticles.^[7] These membranes can simultaneously realize O/W emulsion separation with high efficiency (> 98.5%) and the catalytic degradation for various dye molecules (such as methyl blue, p-nitrophenol) once the polluted water passed through the tortuous internal channels of these membranes. Despite considerable progress, the fatal challenge is the irreversible membrane fouling, which demands repeated and complicated cleaning procedures to keep their initial performances.^[8] Worse still, these procedures inevitably cause not only secondary pollution but also a sharp decline of separation flux and efficiency.^[9] Therefore, it is a pressing need to explore advanced materials with excellent self-cleaning performance to treat multicomponent wastewater effectively.

Recently, graphitic carbon nitride (g-C₃N₄) has generated tremendous attention for designing advanced separation membranes attributing to its inherent merits.^[10] The π - π structure of the g-C₃N₄ can accelerate charge separation and restrain charge recombination. Therefore, it can realize photocatalytic degradation of the pollution under the drive of visible-light irradiation at an appropriate bandgap (2.4–2.8 eV).^[11] Besides, it possesses other superior characteristics, such as stability, nontoxicity,

self-cleaning, and antibacterial properties.^[12] By these advantages, numerous exciting breakthroughs on g-C₃N₄ based membranes have sprung up. For example, Li et al. fabricated a GO-based multifunctional membrane via vacuum-assisted filtration.^[13] Its wettability can be controlled by adjusting the relative dosage of g-C₃N₄ sheets. Dye molecules can be easily adsorbed on the surface of this membrane due to its large specific surface area. Jiang et al. developed a 2D GO/g-C₃N₄@TiO₂ composite membrane through intercalating g-C₃N₄@TiO₂ heterojunctions into GO nanosheets.^[14] The g-C₃N₄ sheets can enlarge the interlayer spacing of GO membrane. Therefore, it can achieve O/W emulsion separation with a flux of 500 L m⁻² h⁻¹ bar⁻¹. Moreover, it displayed a superior self-cleaning ability with a high separation recovery ratio (> 95%) even after cyclic permeations. Recently, Lu et al. fabricated a GO/g-C₃N₄ composite membrane via a self-assembly process.^[15] It presented an outstanding self-cleaning capacity for cyclically separating the O/W emulsion. Despite the significant improvement in the self-cleaning ability of separation membranes, the introduction of g-C₃N₄ sheets often causes a pronounced trade-off between permeation flux and antifouling property.^[16] Furthermore, the photocatalytic efficiency of the g-C₃N₄ sheet-based membrane

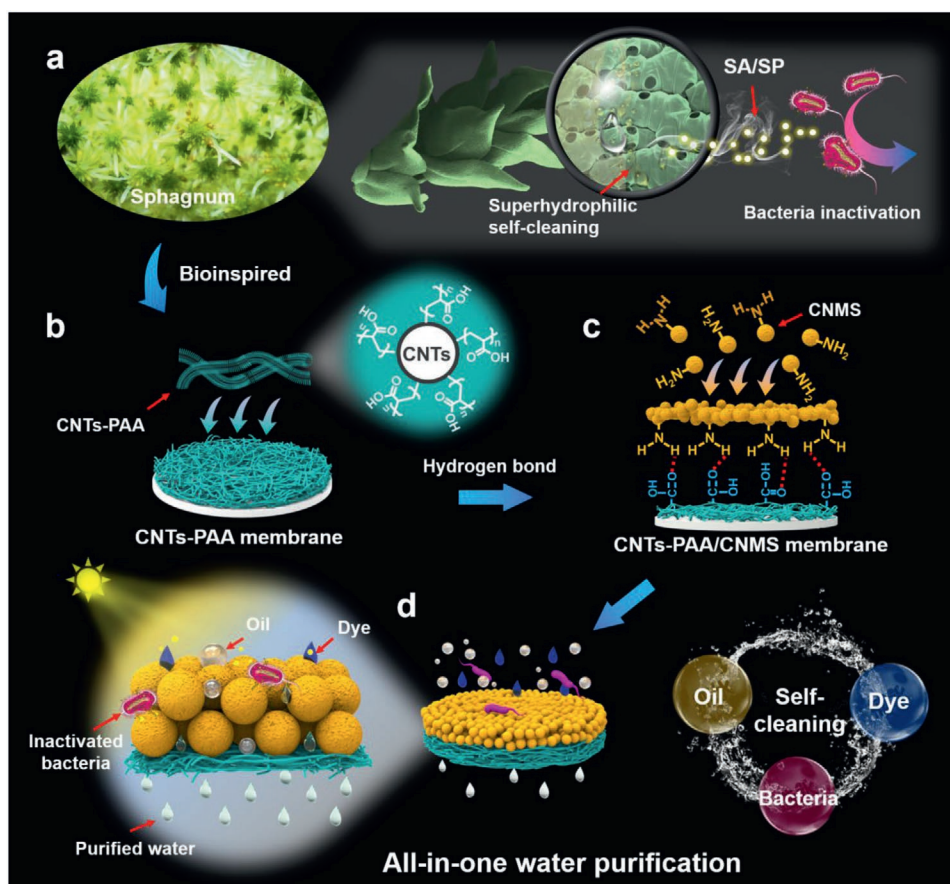


Figure 1. Schematic description of the preparation of CNTs-PAA/CNMS composite membrane with self-cleaning ability for continuous water purification under the drive of sunlight. a) The sphagnum showed self-cleaning and antibacterial properties due to its porous structure and self-secretion of antibacterial substances (sphagnum acid and sphagnum phenol). b) The CNTs was modified with hydrophilic PAA. c) The wrinkled CNMS was assembled on the surface of CNTs-PAA membrane through hydrogen bond and subsequent vacuum filtration. d) The CNTs-PAA/CNMS composite membrane endowed with all-in-one self-cleaning property, which can continuously treat wastewater with multicomponents, including oils, dye molecules, and bacteria.

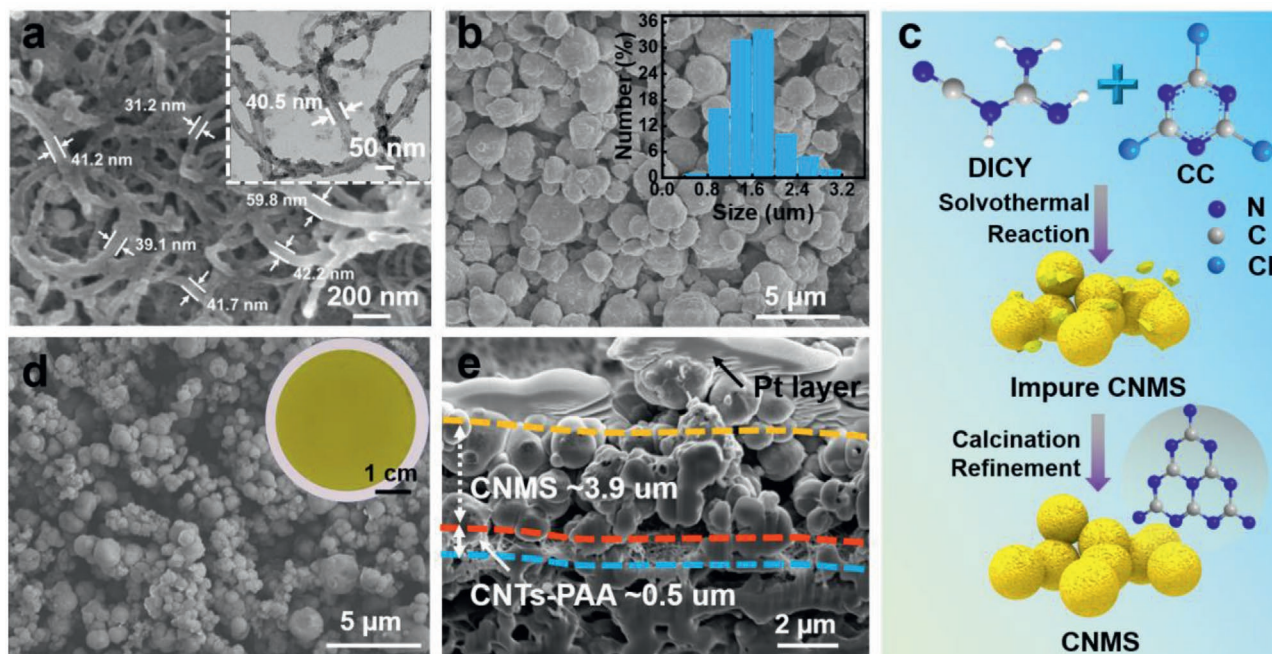


Figure 2. a) The SEM and responding TEM images of CNTs-PAA. b) SEM image and size distribution of the CNMS. c) Schematic illustration of the formation process of CNMS. d) The SEM image and photograph of CNTs-PAA/CNMS composite membrane. e) The cross-sectional SEM image of the CNTs-PAA/CNMS composite membrane.

should be further promoted because of their larger bandgap.^[17] Hence, it is highly anticipated to fully exploit the unmatched features of $g\text{-C}_3\text{N}_4$ to enhance the visible-light sensitivity for realizing the functional integration of separation membrane.

As a magical creator, nature has provided an array of super-wetting surfaces with specific features. For example, sphagnum shows special superhydrophilicity because of its porous structure with a size of 10–20 μm (Figure 1a). It can uptake its gravity 10–25 times that of water. Furthermore, it presents antibacterial ability because it can secrete sphagnum acid (SA) and sphagnum phenol (SP) to effectively inactivate bacteria.^[18] Here, inspired by sphagnum, we have engineered a 0D/2D heterojunction composite membrane by integrating graphitic carbon nitride nanomicrospheres (CNMS) with substantial folding morphology and hydrophilic polyacrylic acid functionalized carbon nanotubes (CNTs-PAA) membrane (Figure 1b,c). Interestingly, the designed CNTs-PAA/CNMS composite membrane can not only separate various O/W emulsions with the maximum flux of $5557 \pm 331 \text{ L m}^{-2} \text{ h}^{-1} \text{ bar}^{-1}$ and the effectiveness of $98.5 \pm 0.6\%$, but also has a superior photocatalytic degradation for dye molecules (with the efficiency of $99.7 \pm 0.2\%$) and antibacterial ability (with the efficiency of $\approx 100\%$). Surprisingly, attributing to its smaller bandgap, this membrane demonstrated an excellent self-cleaning property with stable separation, photocatalytic degradation, and antibacterial performance even after repetitive pollution processes (Figure 1d). Furthermore, it can realize the continuous treatment of contaminated water with multicomponents. These properties will open up new opportunities to construct all-in-one separation materials for simplifying the treatment process of complex wastewater systems.

2. Results and Discussion

2.1. Membrane Structures and Chemical Components

The micromorphology of CNTs membrane and CNTs-PAA membrane was shown in Figure 2a; and Figure S1 (Supporting Information). It can be seen that the diameter of CNTs increased from 24.7 ± 4.6 to 42.5 ± 4.9 nm, which proved that PAA was successfully modified on the CNTs membrane. Furthermore, the micromorphology of CNMS was studied through the scanning electron microscope (SEM). The average size of CNMS was about 1.6 μm (Figure 2b). There were innumerable wrinkles on the surface of CNMS, which was synthesized through solvothermal method (Figure 2c; and Figure S2, Supporting Information). The small size and rough structure of CNMS can promote its effective contact with contaminations. This result was consistent with that of transmission electron microscopy (TEM) (Figure S2, Supporting Information). In addition, the average pore size of CNTs-PPA/CNMS composite membrane was about 0.5 μm (Figure S3, Supporting Information). The chemical composition of CNMS was further tested by the Fourier-transform infrared spectroscopy and Raman spectroscopy (Figure S4, Supporting Information). The broad absorption peak at $3000\text{--}3400 \text{ cm}^{-1}$ was attributed to the stretching of N–H in the surface amino group and C–H on the tri-s-triazine ring (Figure S5a, Supporting Information).^[19] The wide absorption band at $1100\text{--}1700 \text{ cm}^{-1}$ was assigned to aromatic C–N heterocyclic, and the sharp peak at 807 cm^{-1} was corresponding to tri-s-triazine ring units (Figure S5a, Supporting Information).^[19] Figure S5b (Supporting Information) showed the X-ray diffractometer (XRD) curve of CNMS. There

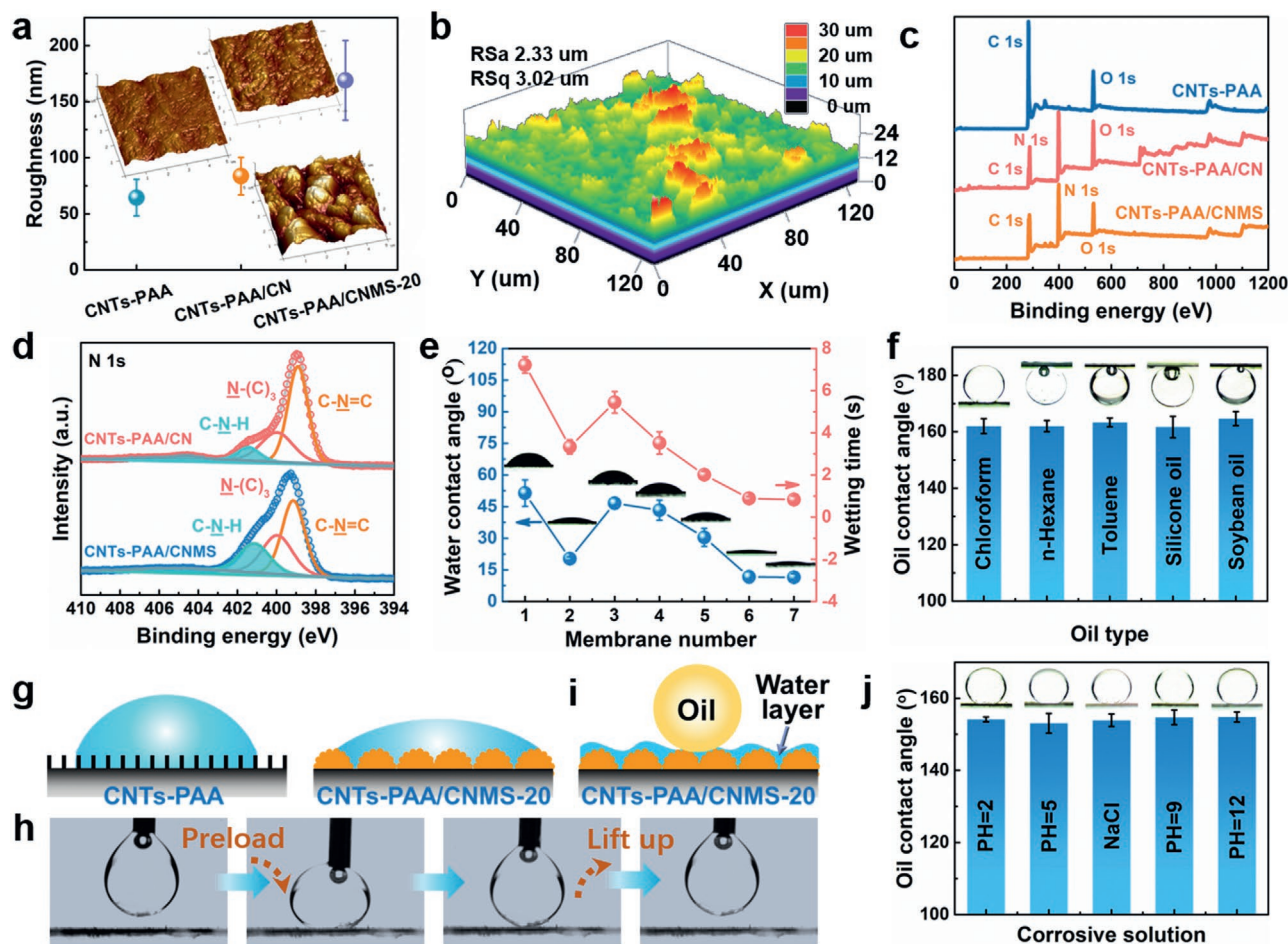


Figure 3. a) The surface roughness of the CNTs-PAA membrane, CNTs-PAA/CN composite membrane, and CNTs-PAA/CNMS composite membrane. b) The CLSM image of CNTs-PAA/CNMS composite membrane. c) The XPS spectra of CNTs-PAA membrane, CNTs-PAA/CN and CNTs-PAA/CNMS composite membranes. d) The N1s spectrum of the CNTs-PAA/CN (upper) and CNTs-PAA/CNMS (down) composite membranes. e) The wettability of each membrane in air (1-CNTs-PAA, 2-CNTs-PAA/CN, 3-CNTs-PAA/CNMS-5, 4-CNTs-PAA/CNMS-10, 5-CNTs-PAA/CNMS-15, 6-CNTs-PAA/CNMS-20, 7-CNTs-PAA/CNMS-25). f) The underwater oil contact angles of the CNTs-PAA/CNMS-20 composite membrane. g) Schematic illustration of the wettability of CNTs-PAA and CNTs-PAA/CNMS-20 composite membrane in air, respectively. h) The underwater oil adhesion process on the CNTs-PAA/CNMS-20 composite membrane. i) Schematic illustration of the oil contact angle underwater of the CNTs-PAA/CNMS-20 composite membrane. j) The contact angles of chloroform underwater on the CNTs-PAA/CNMS-20 composite membranes after being immersed in different corrosion solutions for 72 h.

were two characteristic peaks of $g\text{-C}_3\text{N}_4$ located at 13.6° for (100) reflection and 27.4° for (002) reflection, which was corresponded to the diffraction of the in-plane repeating and graphitic-like aromatic structure, respectively.^[20]

The photograph of sphagnum and its responding SEM image was shown in Figure 1a. It was composed of countless cells that evenly arranged on the inner of sphagnum and formed a porous structure with a size of $\approx 10\text{--}20\ \mu\text{m}$. Therefore, the sphagnum presents hydrophilic capacity. Furthermore, the sphagnum is endowed with antibacterial property due to its cell secretions.^[17] Analogously, the microstructure of CNTs-PAA/CNMS composite membrane was in detail characterized. As displayed in Figure 2d, the CNMS layer (with thickness of $\approx 3.9\ \mu\text{m}$, Figure 2e) was closely packed on the surface of the CNTs-PAA membrane (thickness about $0.5\ \mu\text{m}$, Figure S6, Supporting Information), which was like the cells in the sphagnum. Moreover, the roughness of the CNTs-PAA/CNMS composite

membrane ($169 \pm 35.55\ \text{nm}$) was distinctly far higher than that of the CNTs-PAA membrane ($64.43 \pm 16.19\ \text{nm}$) and polyacrylic acid functionalized carbon nanotubes/graphitic carbon nitride (CNTs-PAA/CN) composite membrane ($83.67 \pm 16.65\ \text{nm}$) (Figure 3a). The enhanced roughness will enhance the visible-light absorptive capacity to decompose pollutants.^[21] This difference was further verified by their responding SEM images and confocal laser scanning microscope (CLSM) images. As shown in Figure 3b; and Figures S7–S8 (Supporting Information), the CNTs-PAA and the CNTs-PAA/CN composite membranes were smoother than that of the obtained CNTs-PAA/CNMS composite membrane. The enhanced roughness can not only increase the effective contact area between the membrane and contaminants but also can improve the absorption capacity of sunlight, which was confirmed by the UV-vis diffuse reflection spectra of these membranes (Figure S9, Supporting Information).

The surface elemental compositions of these membranes were further investigated by X-ray photoelectron spectroscopy (XPS). As shown in Figure 3c, both C 1s and O 1s peaks appeared in the CNTs-PAA, CNTs-PAA/CN, and CNTs-PAA/CNMS composite membranes. The C 1s spectrum could be divided into three peaks at 284.76, 285.18, and 289.99 eV, which were assigned to C=C, C–C, and –COOH, respectively (Figure S10, Supporting Information).^[22] A strong N 1s peak (at ≈ 399 eV) was seen in the XPS spectrum of the CNTs-PAA/CN and CNTs-PAA/CNMS composite membranes. However, there was no N 1s peak in the CNTs-PAA membrane (Figure 3d). The N 1s spectrum can be decomposed into three peaks, which included C–N=C, N–C₃, C–NH₂ at around 399.15, 399.96, 401.12 eV, respectively.^[23] It was worth noting that the hydrophilic C–NH₂ group in the CNTs-PAA/CNMS composite membrane increased to 7.02% in comparison with that of CNTs-PAA/CN composite membrane (3.51%) (Table S1, Supporting Information), which will be favorable to improve the self-cleaning ability of the CNTs-PAA/CNMS composite membrane.

2.2. Surface Wettability

The surface wettability of these composite membranes was also comprehensively investigated through water contact angle (WCA) measurement. The CNTs-PAA membrane showed hydrophilicity with the initial contact angle of $51.4^\circ \pm 6.0^\circ$. It took about 8 s for water (4 μ L) to spread on the surface of this membrane (Movie S1, Supporting Information). However, due to the hydrophilic amino group in g-C₃N₄ sheets, the CNTs-PAA/CN composite membrane was more affinity to water with the original contact angle of $20.3^\circ \pm 0.8^\circ$. The water droplet passed through this membrane within 3 s (Movie S2, Supporting Information). These results indicated the successful modification of g-C₃N₄ sheets on the surface of CNTs-PAA membrane. Furthermore, the surface wettability of CNTs-PAA/CNMS composite membrane changed distinctly along with the volume change of CNMS dispersion. The water droplets inserted into the inner of this membrane within only 1 s when the volume of CNMS dispersion reached to 20 mL (Figure 3e; and Movie S3, Supporting Information). On the one hand, abundant hydrophilic functional groups (e.g., –COOH and –NH₂) on the surface of the CNTs-PAA/CNMS-20 composite membrane endowed it with good affinity with water.^[24] On the other hand, according to Wenzel mode, the roughness produced by the CNMS hierarchical structure made the hydrophilic interface more hydrophilic.^[25] These resulted in accelerating the diffusion and penetration of water droplets (Figure 3g). In addition, this membrane demonstrated underwater superoleophobicity with oil contact angle all greater than 150° (Figure 3f). The oil droplets can be rapidly detached from the CNTs-PAA/CNMS-20 composite membrane once it was contacted with its surface (Figure 3h). The special wettability of the CNTs-PAA/CNMS-20 composite membrane was mainly attributed to its chemical composition and interface morphology.^[26] Due to its superhydrophilicity, the CNTs-PAA/CNMS-20 composite membrane was completely infiltrated by water and formed a continuous water layer at the air/water/solid three-phase interface, which resulted in the reduction of the effective contact area between the oil phase and the membrane surface (Figure 3i).^[27] The

wetting stability of CNTs-PAA/CNMS-20 composite membrane was further studied by immersing it into the hydrochloric acid (HCl), sodium hydroxide (NaOH), and sodium chloride (NaCl, 35 g L⁻¹) solutions for 72 h, respectively. As demonstrated in Figure 3j, there were almost no changes even being corroded under these harsh environments, indicating the excellent chemical adaptability of the CNTs-PAA/CNMS-20 membrane.

2.3. Emulsion Separation and Self-Cleaning Performance

The particular wettability made the CNTs-PAA/CNMS-20 heterojunction membrane a promising material for emulsion separation. Here, chloroform-in-water (C/W) emulsion was selected as a representative O/W emulsion to evaluate its separation capacity. As shown in Figure 4a, the CNTs-PAA membrane presented a high separation flux (1960 ± 114 L m⁻² h⁻¹ bar⁻¹) for C/W emulsion with the efficiency of $94.3 \pm 0.5\%$. However, after the modification with g-C₃N₄ sheets or CNMS, their separation efficiencies improved to $98.3 \pm 0.5\%$ and $98.5 \pm 0.6\%$, respectively in despite of a slight drop of separation flux. Notably, the separation flux of CNTs-PAA/CNMS-20 composite membrane (1960 ± 82 L m⁻² h⁻¹ bar⁻¹) was higher than that of the CNTs-PAA/CN (1465 ± 30 L m⁻² h⁻¹ bar⁻¹) composite membrane. This was ascribed to the accumulation of CNMS on the membrane surface, providing more water channels than g-C₃N₄ sheets with stacking structure. Dynamic light scattering measurement was also carried out to qualitatively analyze the separation ability of the CNTs-PAA/CNMS-20 composite membrane. As displayed in Figure 4b; and Figure S11 (Supporting Information), the feed emulsion showed a milky white with a size of ≈ 120 nm. In comparison, the filtrate was almost transparent and not any droplets can be observed. These results have been further proved through optical microscopy (Figure S11, Supporting Information). In addition, the stability of the CNTs-PAA/CNMS-20 composite membrane was evaluated by performing cyclic separations for C/W emulsion. As displayed in Figure 4c, the separation performance did not display remarkable change after sixteen cycles of separation process. Similar results were also achieved for other emulsions (Figure 4d; and Figures S12 and S13, Supporting Information), including methylene chloride-in-water (M/W) emulsion, hexane-in-water (H/W) emulsion, toluene-in-water (T/W) emulsion, silicone oil-in-water (Si/W) emulsion, soybean oil-in-water (So/W) emulsion. They have displayed excellent separation flux with of 1750 ± 20 , 4468 ± 292 , 5557 ± 331 , 1700 ± 36 , and 3761 ± 32 L m⁻² h⁻¹ bar⁻¹, respectively.

The emulsion separation mechanism of CNTs-PAA/CNMS-20 heterojunction membrane was deduced as follows. This membrane was hydrophilic in the air, so the water phase can spread on its surface spontaneously and formed a water layer due to the capillary effect ($\Delta P < 0$) from its hydrophilic pores.^[26,28] Moreover, the CNTs-PAA/CNMS-20 composite membrane showed oil-repellent property with an underwater oil contact angle above 150° . In this case, the demulsification phenomenon occurred once the emulsion touching with the CNTs-PAA/CNMS-20 composite membrane.^[29] The water droplets agglomerated and passed across the CNTs-PAA/CNMS-20 composite membrane but the oil was restricted (Figure 4e).

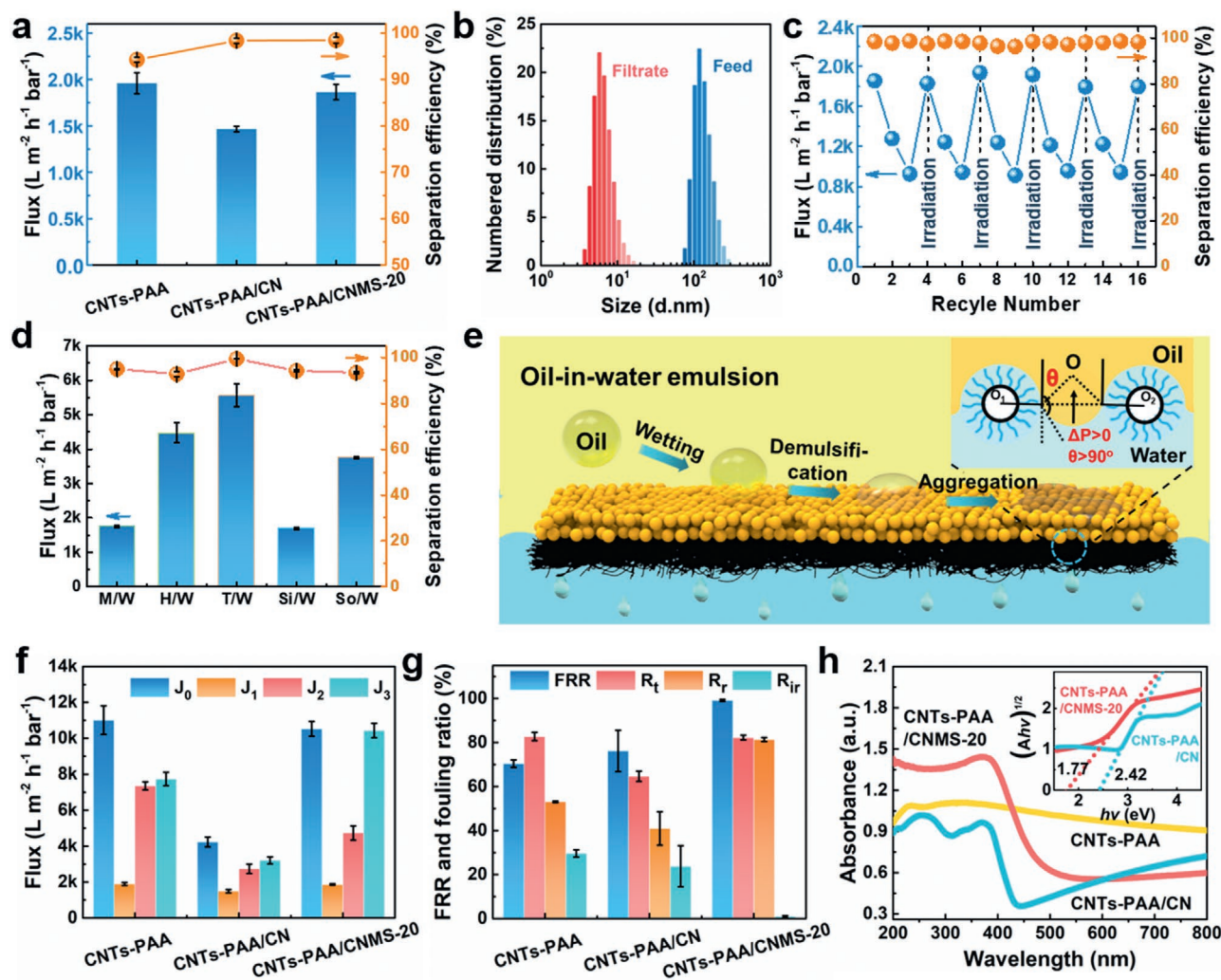


Figure 4. a) Separation efficiency and flux of each membrane for C/W emulsion. b) The oil droplet size in the feed and filtration of the C/W emulsion. c) The flux and separation efficiency of the CNTs-PAA/CNMS-20 composite membrane during cyclic emulsion separation. d) The separation ability of the CNTs-PAA/CNMS-20 composite membrane for various O/W emulsions. e) Schematic of demulsification mechanism for O/W emulsion. f) The initial and recovery flux of the CNTs-PAA membrane, CNTs-PAA/CN composite membrane and CNTs-PAA/CNMS-20 composite membrane, respectively. (J_0 : initial flux, J_1 : water flux after emulsion separation, J_2 : water flux after being washed with water, J_3 : water flux after being irradiated under sunlight). g) The flux recovery ratio (FRR), the total fouling ratio (R_t), irreversible fouling ratio (R_{ir}), and reversible fouling ratio (R_r) of the CNTs-PAA, CNTs-PAA/CN, and CNTs-PAA/CNMS-20 composite membranes, respectively. h) UV-vis absorption spectra of CNTs-PAA, CNTs-PAA/CN, and CNTs-PAA/CNMS-20 composite membranes, respectively (Inset: the plots of $(\Delta hv)^{1/2}$ vs hv of the CNTs-PAA/CNMS-20 and CNTs-PAA/CN composite membranes).

The antifouling performance is a key index to assess the comprehensive performance of membrane separation materials for practical application.^[30] The self-cleaning ability of the CNTs-PAA/CNMS-20 composite membrane was studied by calculating the water flux before and after C/W emulsion separation. As shown in Figure S14 (Supporting Information), there was a lot of oil pollutants adsorbed on the surface of the CNTs-PAA/CNMS-20 composite membrane. However, after irradiated under sunlight, this membrane has recovered to initial structure, which indicated the excellent the sunlight absorption and self-cleaning ability of this membrane. Furthermore, the initial water flux (J_0) of the CNTs-PAA, CNTs-PAA/CN, and CNTs-PAA/CNMS-20 composite membranes were $11\,000 \pm 791$, 4200 ± 270 , and $10\,500 \pm 413$ L m⁻² h⁻¹ bar⁻¹, respectively (Figure 4f). During the emulsion separation process, the water

flux (J_1) of these membranes has sharply declined to 2010 ± 70 , 1650 ± 20 , and 1899 ± 65 L m⁻² h⁻¹ bar⁻¹, respectively. This was due to the aggregation and adhesion of oil droplets on the membrane surface. After alternative cleaning with water and ethanol, the water flux (J_2) of these membranes have recovered to 7000 ± 227 , 2700 ± 259 , and 4700 ± 396 L m⁻² h⁻¹ bar⁻¹, respectively. Interestingly, with regard to CNTs-PAA membrane and CNTs-PAA/CN composite membrane, after the irradiation with sunlight, their recovery water flux (J_3) have only increased to 7741 ± 371 , 3208 ± 196 L m⁻² h⁻¹ bar⁻¹, respectively. These results suggested the lower self-cleaning property of CNTs-PAA and CNTs-PAA/CN composite membranes. On the contrary, the recovery water flux of CNTs-PAA/CNMS-20 composite membrane was attained to $10\,436 \pm 397$ L m⁻² h⁻¹ bar⁻¹ just under the drive of sunlight (Figure 4f). Furthermore, the fouling ratio

of these membranes was evaluated by calculating the change of separation flux before and after emulsion separation. It can be seen that the total fouling ratio (R_t) of CNTs-PAA, CNTs-PAA/CN, and CNTs-PAA/CNMS-20 composite membranes were $82.7 \pm 1.9\%$, $64.7 \pm 2.4\%$, and $82.2 \pm 1.1\%$, respectively. However, the water flux recovery ratio (FRR) of CNTs-PAA/CNMS-20 composite membrane ($99.5 \pm 0.5\%$) was larger than that of the CNTs-PAA membrane ($70.4 \pm 1.6\%$), CNTs-PAA/CN composite membrane ($76.2 \pm 9.3\%$) (Figure 4g). In addition, the CNTs-PAA/CNMS-20 composite membrane revealed the lowest irreversible fouling ratio (R_{ir}) of $0.8 \pm 0.4\%$ and the highest reversible fouling ratio (R_r) of $81.3 \pm 0.9\%$ compared with that of the CNTs-PAA membrane ($R_{ir} = 29.7 \pm 1.6\%$, $R_r = 50.2 \pm 0.4\%$) and CNTs-PAA/CN composite membrane ($R_{ir} = 23.8 \pm 9.4\%$, $R_r = 41.0 \pm 7.6\%$) (Figure 4g). The excellent self-cleaning ability of the CNTs-PAA/CNMS-20 composite membrane was attributed to the synergetic effect of special wettability and the photocatalytic degradation property of g-C₃N₄. On the one hand, the hydrophilic functional groups (–COOH, –NH₂) can effectively prevent oil from adhering to its inner/outer surface. On the other hand, the absorption band edges of the CNTs-PAA/CNMS-20 and CNTs-PAA/CN composite membrane were different in the visible-light region from 400 to 550 nm. The absorption edge of CNTs-PAA/CNMS-20 composite membrane presented a redshift compared with that of the CNTs-PAA/CN composite membrane (Figure 4h). This result was due to the high condensation degree of CNMS, which can be proved by XRD.^[31] This difference endowed the CNTs-PAA/CNMS-20 composite membrane with enhanced visible-light absorptive capacity to decompose pollutants. Moreover, the CNTs-PAA/CNMS-20 composite membrane (1.77 eV) has a smaller bandgap than that of CNTs-PAA/CN composite membrane (2.42 eV) (Figure 4h), which was mainly due to the improvement of inter-planar accumulation and electron delocalization of the J-type aggregates during the solvothermal process.^[31]

2.4. Photocatalytic Degradation Performance

Photocatalytic degradation is thought of as the most practicable means to eliminate water-soluble pollutants.^[31] RhB was chosen as a representative dye molecule to assess the photocatalytic degradation ability of the CNTs-PAA/CNMS heterojunction membrane under visible-light ($\lambda > 420$ nm). As presented in Figure 5a, the CNTs-PAA/CNMS composite membrane demonstrated higher photocatalytic activity than that of the CNTs-PAA membrane and CNTs-PAA/CN composite membrane. Moreover, with the increasing volume of CNMS dispersion, the photocatalytic degradation capacity increased until it came up to $99.7 \pm 0.2\%$. Excessive dosage of CNMS may bring about agglomeration and even accumulation phenomena, which resulted in lower photocatalytic efficiency. The photocatalytic activities of these composite membranes were further determined by a pseudo-first-order kinetic equation with a linear fit of $\ln(C_0/C)$ against time. It can be revealed that there was a three-stage kinetics process of CNTs-PAA/CNMS-20 composite membrane during the photocatalytic degradation process of RhB (Figure 5b). Besides, the photodegradation rate increased along with the irradiation time. This was because

the decoloration of RhB can decrease the reflection and refraction of incident sunlight on the dye solution.^[32] The CNTs-PAA/CNMS-20 composite membrane can receive stronger irradiation intensity and further increase the reaction rate. Remarkably, the maximum photodegradation rate constant of CNTs-PAA/CNMS-20 composite membrane for RhB reached 0.0736 min^{-1} in the third stage (0.0168 min^{-1} in the first stage and 0.0376 min^{-1} in the second stage), which were 14 and 26 times than that of CNTs-PAA/CN (0.0050 min^{-1}) and CNTs-PAA (0.0028 min^{-1}) membrane, respectively.

Furthermore, we studied the photocatalytic degradation capacity of these membranes by UV-vis spectrophotometer. As shown in Figure 5c, the intensity of the maximum absorption peak (RhB, $\lambda_{\text{max}} = 554$ nm) of the CNTs-PAA membrane declined with the extension of irradiation time. Moreover, there was no shift of the maximum absorption wavelength and each absorption curve was almost parallel to each other. This indicated that there was only the adsorption process of the CNTs-PAA membrane for RhB. As to CNTs-PAA/CN composite membrane, it has displayed a blueshift of the λ_{max} of RhB, which revealed that the photocatalytic reaction has occurred on the membrane surface and the by-products were generated. For CNTs-PAA/CNMS-20 composite membrane, its λ_{max} has gradually shifted from the initial 554 nm toward shorter wavelength, eventually reaching 497 nm. This phenomenon of the CNTs-PAA/CNMS-20 composite membrane was associated with the N-de-ethylation process, which included RhB (≈ 554 nm), N, N, N'-tri-ethylated rhodamine (≈ 539 nm), N, N'-di-ethylated rhodamine (≈ 522 nm), N-ethylated rhodamine (≈ 510 nm), and de-ethylated rhodamine (≈ 497 nm).^[33] Simultaneously, the conjugate structure of rhodamine was broken down into small molecules upon continuous visible-light irradiation.^[34] The stability of the CNTs-PAA/CNMS-20 heterojunction membrane was further assessed by monitoring the cyclic photocatalytic degradation for RhB. As presented in Figure 5d, the CNTs-PAA/CNMS-20 composite membrane maintained its outstanding photocatalytic degradation performance ($> 90\%$) after ten cycle's experiments, suggesting that the CNTs-PAA/CNMS-20 composite membrane can keep an efficient photocatalytic activity in long-term use. Besides that, this membrane can be used for degrading other dye molecules, such as methyl blue (MB), malachite green (MG) with the efficiency of 98.8%, 95.3%, respectively (Figures S15 and S16, Supporting Information), which further indicated its potential application value in wastewater treatment. The photocatalytic degradation mechanism of the CNTs-PAA/CNMS-20 composite membrane for dye molecules can be deduced as the following equations^[35]



During the photocatalysis process, the CNMS can stimulate a $\pi \rightarrow \pi^*$ electronic transition by absorbing photon energy ($h\nu$) under the condition that it is larger than the energy gap

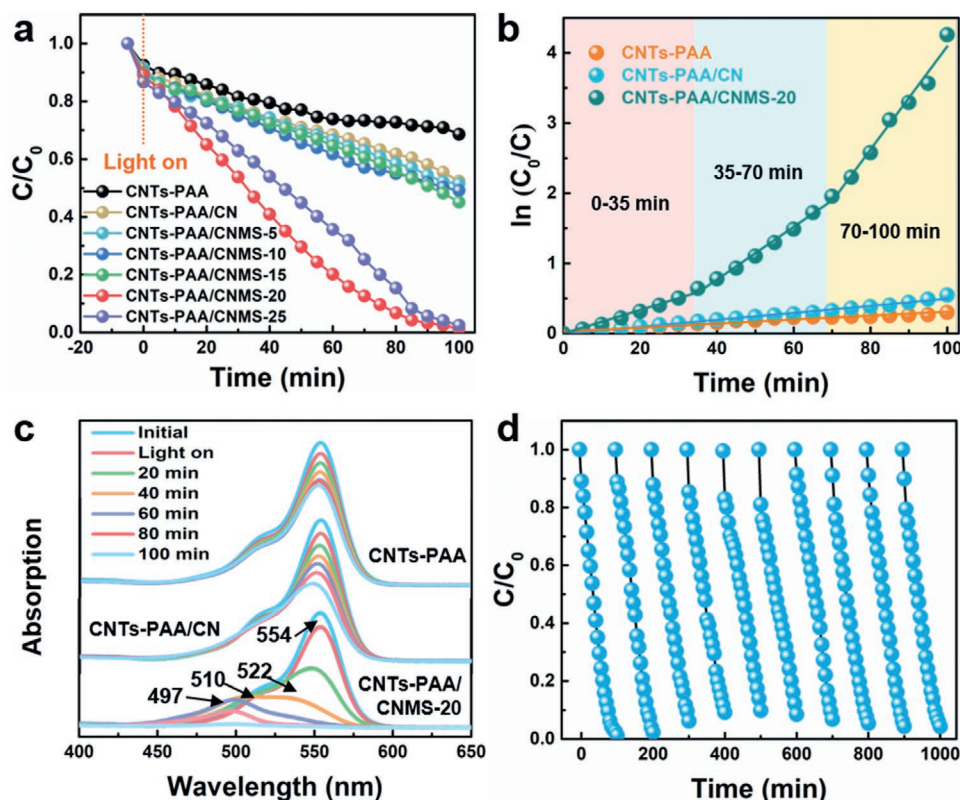


Figure 5. a) Photocatalytic activities of CNTs-PAA membrane, CNTs-PAA/CN composite membrane, and CNTs-PAA/CNMS composite membranes with different amounts of CNMS for RhB. b) Photocatalytic rates of the CNTs-PAA membrane, CNTs-PAA/CN composite membrane, and CNTs-PAA/CNMS-20 composite membrane for RhB. c) UV-vis absorption spectra for RhB solution after being treated with CNTs-PAA membrane, CNTs-PAA/CN membrane, and CNTs-PAA/CNMS-20 membrane under sunlight. d) Cycling photocatalytic performance of CNTs-PAA/CNMS-20 composite membrane for RhB solution.

of CNMS (Equation (1)). The produced photoinduced electrons (e^-) will transfer from its valence band (VB) across the forbidden band to the conduction band (CB). In contrast, the photoinduced positive holes (h^+) are left its conduction band. Subsequently, the e^- and h^+ will migrate to different positions of CNMS under electric field. Lastly, the h^+ will directly oxidize pollutants adsorbed on the surface of $g-C_3N_4$ into CO_2 and H_2O (Equation (2)). Moreover, the e^- will reduce O_2 into highly active O_2^- , which will undergo redox reactions with organic pollutants adsorbed on the CNMS layer and eventually degrade these contaminations into CO_2 and H_2O (Equations (3) and (4)).

2.5. Photocatalytic Antibacterial Performance

$g-C_3N_4$ has received increasing attention owing to its photoinduced sterilization ability.^[36] As a typical waterborne bacterium, *Escherichia coli* (*E. coli*) was selected to evaluate the antibacterial performance of CNTs-PAA/CNMS-20 composite membrane. As depicted in Figure 6a,b, the CNTs-PAA membrane exhibited lower antibacterial efficiency ($38.29 \pm 8.0\%$) due to its poor visible-light response. After being modified with $g-C_3N_4$ sheets, the antibacterial ability of the CNTs-PAA/CN composite membrane increased to $70.92 \pm 7.0\%$. This remarkable change was attributed to the absorption capacity of the sunlight in the visible spectra range of $g-C_3N_4$ sheets (2.42 eV). Surprisingly, the

CNTs-PAA/CNMS-20 composite membrane presented better antibacterial ability than that of the CNTs-PAA/CN composite membrane. As shown in Figure 6a–d, almost all the bacteria, such as *E. coli*, *Staphylococcus aureus* (*S. aureus*), and *Proteus mirabilis* (*P. mirabilis*), lost their activities within 2 h after the photocatalytic antibacterial process of the CNTs-PAA/CNMS-20 composite membrane. For one thing, this superior performance came from the inherent antibacterial property of $g-C_3N_4$.^[37] First, the bacteria adhered to the surface of the CNTs-PAA/CNMS-20 composite membrane. Second, under the illumination of sunlight, the CNMS produced reactive oxygen species, such as hydroxyl radicals and superoxide radicals, which can directly induce the cellular constituent oxidation.^[35,38] Finally, the bacterial cell wall was destroyed and the living substances leakage from the cell inside, which resulted in the inactivation of bacteria (Figure 6e). For another, the rough micromorphology came from the CNMS brought more active sites and produce more active O_2^- , which was conducive to accelerate the inactivation of bacteria.^[38] In addition, its excellent hydrophilicity was beneficial to the effective contact between bacteria and membrane surface.^[39]

2.6. All-in-One Water Purification

The purification of actual domestic sewage remains a very challenging task because there are thousands of hazardous

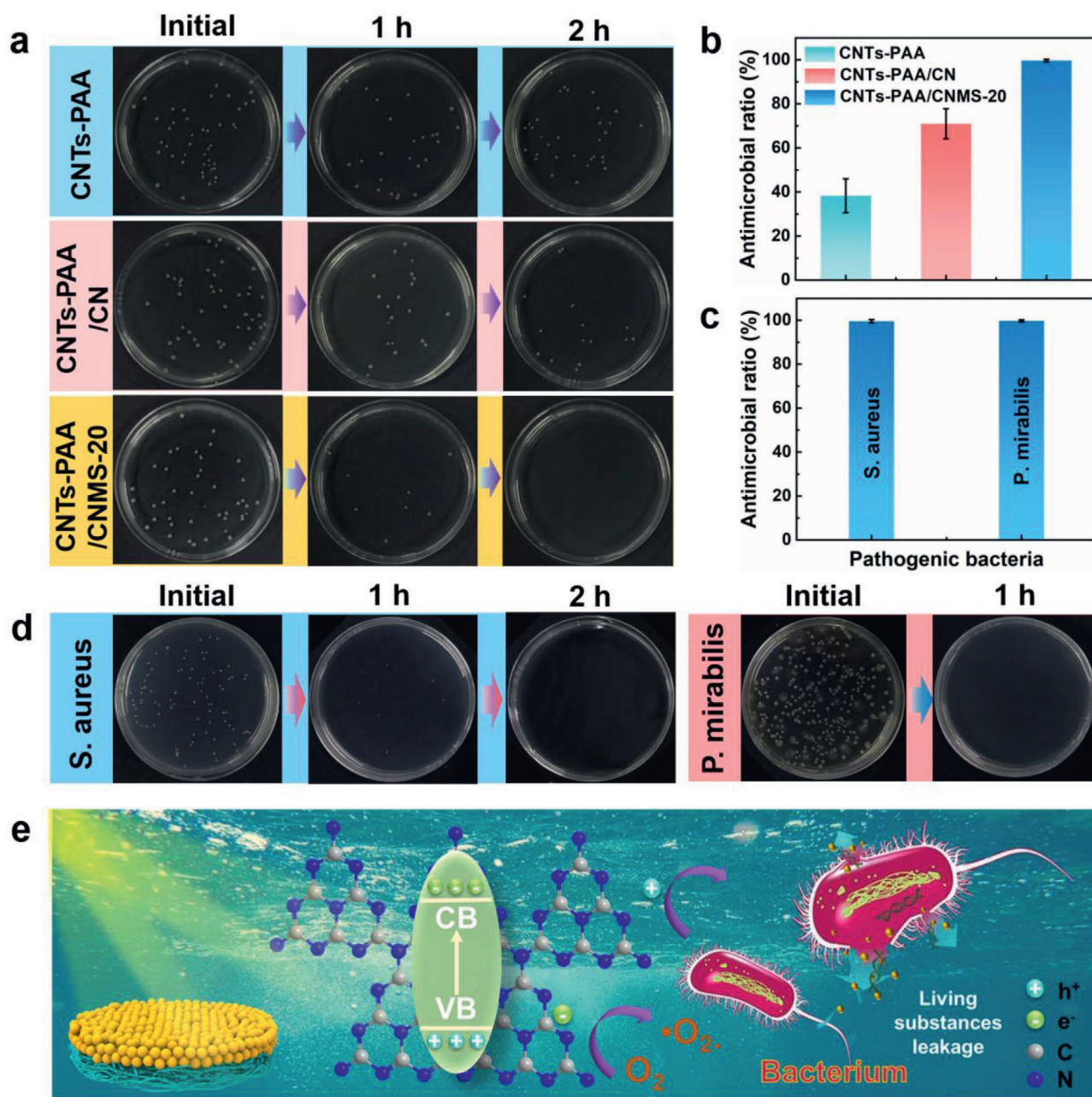


Figure 6. a) Photographs of the photocatalytic antibacterial effects of the CNTs-PAA membrane, CNTs-PAA/CN composite membrane, and CNTs-PAA/CNMS-20 heterojunction membrane against *E. coli*, respectively. b) The photocatalytic antibacterial efficiency of the CNTs-PAA membrane, CNTs-PAA/CN composite membrane, and CNTs-PAA/CNMS-20 heterojunction membrane, respectively. c) The photocatalytic antibacterial efficiency of the CNTs-PAA/CNMS-20 heterojunction membrane for *S. aureus* and *P. mirabilis*. d) Photographs of the antibacterial effects of CNTs-PAA/CNMS-20 heterojunction membrane against *S. aureus* and *P. mirabilis*, respectively. e) Photocatalytic antibacterial mechanism of the CNTs-PAA/CNMS-20 heterojunction membrane.

compounds in polluted water. The continuous sewage treatment ability of the CNTs-PAA/CNMS-20 composite membrane was further explored to evaluate its potential application value. It included three steps (Figure 7a). First, the CNTs-PAA/CNMS-20 composite membrane was applied to purify the wastewater containing bacteria. As displayed in Figure 7b,c, this membrane can completely inactivate the bacteria under the irradiation of sunlight within 2 h. Moreover, this membrane kept its initial macromorphology without visible loss.

Second, the CNTs-PAA/CNMS-20 composite membrane, after being used for the antibacterial experiment, was applied to separate C/W emulsion. It can be seen that the permeation flux drastically decreased to $710 \pm 42 \text{ L m}^{-2} \text{ h}^{-1} \text{ bar}^{-1}$ after three times of separation even though the separation efficiency still remained above 98.2%. This dramatic change was due to the membrane fouling coming from the collective effect of the dead bacteria and demulsified oil. They can block the separation channel and increase mass transfer resistance.

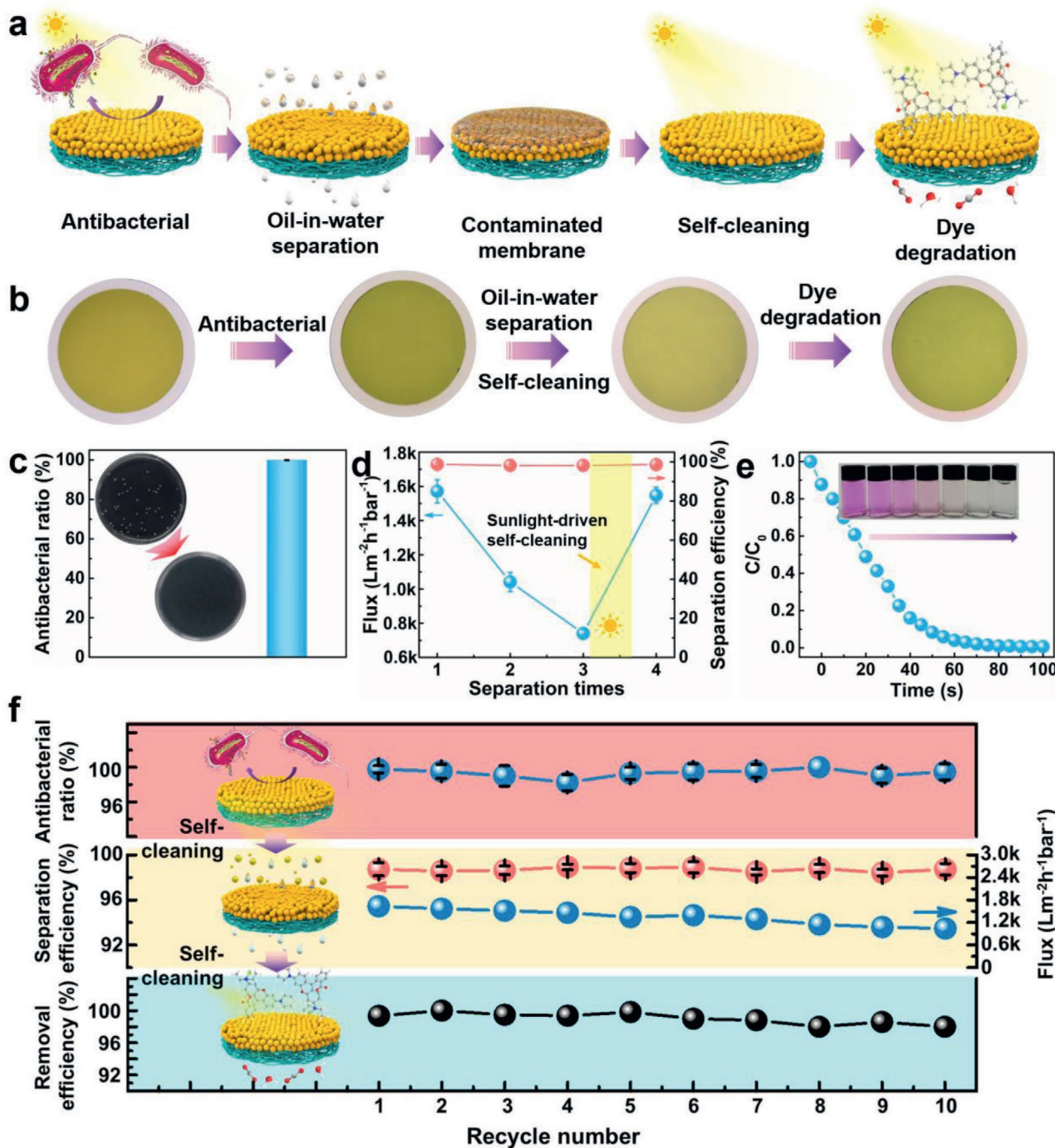


Figure 7. a) The continuous water environment optimization process of the CNTs-PAA/CNMS-20 composite membrane, including antibacteria, emulsion separation, dye degradation, and self-cleaning. b) Photographs of the CNTs-PAA/CNMS-20 composite membrane at different stages. c) The antibacterial ability of the CNTs-PAA/CNMS-20 composite membrane in the first stage. d) The self-cleaning and emulsion separation capacity of this membrane after the treatment of sunlight in the second stage. e) Photocatalytic degradation performance of the CNTs-PAA/CNMS-20 composite membrane for RhB under the irradiation of sunlight in the last stage. f) The cyclic self-cleaning and purification process of the CNTs-PAA/CNMS-20 composite membrane.

Nevertheless, the separation flux of the C/W emulsion can be recovered to $1548 \pm 49 \text{ L m}^{-2} \text{ h}^{-1} \text{ bar}^{-1}$ and the separation efficiency kept $98.6 \pm 0.8\%$ only under the illumination of sunlight. These demonstrated the splendid sunlight-driven self-cleaning ability of the CNTs-PAA/CNMS-20 composite

membrane (Figure 7d). Finally, the treated membrane was further employed as a photocatalytic material to purify the polluted water containing RhB. Encouragingly, it still maintained its excellent photocatalytic degradation performance for dye molecules with an efficiency of $99.3 \pm 0.6\%$

(Figure 7e). Notably, the CNTs-PAA/CNMS-20 composite membrane possessed stable water purification capability after a multistep and continuous separation process (Figure 7f; and Figures S17–S19, Supporting Information). At the same time, there were no obvious morphological changes during the all-in-one purification cycles, which proved excellent mechanical stability of the CNTs-PAA/CNMS-20 composite membrane (Figure S20, Supporting Information). The excellent comprehensive performance of the CNTs-PAA/CNMS-20 composite membrane (Table S2, Supporting Information) will make it a promising material to simultaneously remove coexisting contaminations in water.

3. Conclusion

In summary, an all-in-one CNTs-PAA/CNMS composite membrane has been presented by imitating the hierarchical structure and functions of sphagnum. The joint effect of hydrophilic CNTs-PAA and CNMS with wrinkled structure endowed this membrane with the superior overall performance for water purification. To be specific, this membrane can not only separate various O/W emulsions with the maximum flux up to $5557 \pm 311 \text{ L m}^{-2} \text{ h}^{-1} \text{ bar}^{-1}$ and the efficiency of $98.5 \pm 0.6\%$, but also can realize the catalytic degradation for various dye molecules with the efficiency of $99.7 \pm 0.2\%$ and antibacterial ability with the ratio close to 100%. Remarkably, it presented outstanding self-cleaning ability attributing to its smaller bandgap (1.77 eV), which was smaller than that of the traditional $\text{g-C}_3\text{N}_4$ sheets-based photocatalytic membrane. Therefore, it can continuously purify multicomponent wastewater without any loss of performance. This work may open up a door to develop advanced materials with multifunctional integration to restore the water environment.

Supporting Information

Supporting Information is available from the Wiley Online Library or from the author.

Acknowledgements

L.T.J. and L.K.Y. contributed equally to this work. The authors would like to thank to Dr. Hang Guo, Miss. Yu Wang, and Prof. Lingjie Meng at the Instrumental Analysis Center of Xi'an Jiaotong University for their assistance with characterizations. This work was supported by the Fundamental Research Funds for the National Key Research and Development Program of China (Nos. 2019YFC1606600 and 2019YFC1606603), Central Universities, CHD (Nos. 300102318403, 300102319306, and 300102310104), and Shaanxi Key Research and Development Project (No. 2020ZDLGY13-08), Xi'an Science and Technology Bureau Science and technology Innovation Talent Service Enterprise Project (No. 2020KJRC0127), K. C. Wong Education Foundation (GJTD-2019-13).

Conflict of Interest

The authors declare no conflict of interest.

Data Availability Statement

The data that support the findings of this study are available from the corresponding author upon reasonable request.

Keywords

$\text{g-C}_3\text{N}_4$ nano/microspheres, self-cleaning property, smaller bandgap, sunlight-driven water purification, superhydrophilicity

Received: November 16, 2020

Revised: December 30, 2020

Published online: February 15, 2021

- [1] a) J. J. Li, Y. N. Zhou, Z. H. Luo, *Prog. Polym. Sci.* **2018**, *87*, 1; b) Y. H. Guo, H. Y. Lu, F. Zhao, X. Zhou, W. Shi, G. Yu, *Adv. Mater.* **2020**, *32*, 1907061; c) G. Q. Shen, L. Pan, R. R. Zhang, S. C. Sun, F. Hou, X. W. Zhang, J. J. Zou, *Adv. Mater.* **2020**, *32*, 1905988; d) Y. Q. Zhang, X. Q. Cheng, X. Jiang, J. J. Urban, C. H. Lau, S. Q. Liu, L. Shao, *Mater. Today* **2020**, *36*, 40.
- [2] a) N. A. Khan, R. N. Zhang, H. Wu, J. L. Shen, J. Q. Yuan, C. Y. Fan, L. Cao, M. A. Olson, Z. Y. Jiang, *J. Am. Chem. Soc.* **2020**, *142*, 13450; b) H. E. Karahan, K. Goh, C. F. Zhang, E. Yang, C. Yildirim, C. Y. Chuah, M. G. Ahunbay, J. Lee, Ş. B. Tantekin-Ersolmaz, Y. Chen, T. H. Bae, *Adv. Mater.* **2020**, *32*, 1906697; c) W. Wang, X. W. Du, H. Vahabi, S. Zhao, Y. M. Yin, A. K. Kota, T. Z. Tong, *Nat. Commun.* **2019**, *10*, 3220; d) Y. Kang, Y. Xia, H. T. Wang, X. W. Zhang, *Adv. Funct. Mater.* **2019**, *29*, 1902014; e) Z. J. Xie, Y. P. Peng, L. Yu, C. Y. Xing, M. Qiu, J. Q. Hu, H. Zhang, *Sol. RRL* **2020**, *4*, 201900400.
- [3] a) Y. Choi, S. S. Kim, J. H. Kim, J. Kang, E. Choi, S. E. Choi, J. P. Kim, O. Kwon, D. W. Kim, *ACS Nano* **2020**, *14*, 12195; b) M. C. Zhang, K. C. Guan, Y. F. Ji, G. P. Liu, W. Q. Jin, N. P. Xu, *Nat. Commun.* **2019**, *10*, 1253; c) G. P. Liu, W. Q. Jin, *Sci. China Mater.* **2018**, *61*, 1021.
- [4] a) Z. L. Chu, Y. J. Feng, S. Seeger, *Angew. Chem., Int. Ed.* **2015**, *54*, 2328; b) J. Ge, H. Y. Zhao, H. W. Zhu, J. Huang, L. A. Shi, S. H. Yu, *Adv. Mater.* **2016**, *28*, 10459; c) H. B. Huang, H. D. Shi, P. Das, J. Q. Qin, Y. G. Li, X. Wang, F. Su, P. C. Wen, S. Y. Li, P. F. Lu, F. Y. Liu, Y. J. Li, Y. Zhang, Y. Wang, Z. S. Wu, H. M. Cheng, *Adv. Funct. Mater.* **2020**, *30*, 1909035.
- [5] a) R. X. Qu, X. Y. Li, W. F. Zhang, Y. N. Liu, H. J. Zhai, Y. Wei, L. Feng, *J. Mater. Chem. A* **2020**, *8*, 7677; b) H. Yu, Y. He, G. Q. Xiao, Y. Fan, J. Ma, Y. X. Gao, R. T. Hou, X. Y. Yin, Y. Q. Wang, X. Mei, *Chem. Eng. J.* **2020**, *389*, 124375; c) Y. B. Yang, X. D. Yang, L. Liang, Y. Y. Gao, H. Y. Cheng, X. M. Li, M. C. Zou, A. Y. Cao, R. Z. Ma, Q. Yuan, X. F. Duan, *Science* **2019**, *364*, 1057.
- [6] Y. Liu, F. R. Zhang, W. X. Zhu, D. Su, Z. Y. Sang, X. Yan, S. Li, J. Liang, S. X. Dou, *Carbon* **2020**, *160*, 88.
- [7] a) L. Zhang, J. C. Gu, L. P. Song, L. Chen, Y. J. Huang, J. W. Zhang, T. Chen, *J. Mater. Chem. A* **2016**, *4*, 10810; b) L. K. Yan, G. Zhang, L. Zhang, W. Zhang, J. C. Gu, Y. J. Huang, J. W. Zhang, T. Chen, *J. Membr. Sci.* **2019**, *569*, 32; c) C. H. Liu, J. Y. Xia, J. C. Gu, W. Q. Wang, Q. Q. Liu, L. K. Yan, T. Chen, *J. Hazard. Mater.* **2021**, *403*, 123547.
- [8] a) A. T. Xie, J. Y. Cui, J. Yang, Y. Y. Chen, J. D. Dai, J. H. Lang, C. X. Li, Y. S. Yan, *J. Mater. Chem. A* **2019**, *7*, 8491; b) Y. B. Wei, Y. X. Zhu, Y. J. Jiang, *Chem. Eng. J.* **2019**, *356*, 915.
- [9] Y. Z. Zhu, J. L. Wang, F. Zhang, S. J. Gao, A. Q. Wang, W. X. Fang, J. Jin, *Adv. Funct. Mater.* **2018**, *28*, 1804121.
- [10] a) P. P. Shao, R. X. Yao, G. Li, M. X. Zhang, S. Yuan, X. Q. Wang, Y. H. Zhu, X. M. Zhang, L. Zhang, X. Feng, B. Wang, *Angew. Chem., Int. Ed.* **2020**, *59*, 4401; b) Y. Wang, N. N. Wu, Y. Wang, H. Ma, J. X. Zhang, L. L. Xu, M. K. Albolqany, B. Liu, *Nat. Commun.* **2019**, *10*, 2500.

- [11] a) Y. Wang, H. Wang, J. Li, X. Zhao, *Appl. Catal. B: Environ.* **2020**, 278, 118981; b) J. Barrio, M. Volokh, M. Shalom, *J. Mater. Chem. A* **2020**, 8, 11075.
- [12] a) F. L. Wang, Y. P. Feng, P. Chen, Y. F. Wang, Y. H. Su, Q. X. Zhang, Y. Q. Zeng, Z. J. Xie, H. J. Liu, Y. Liu, W. Y. Lv, G. G. Liu, *Appl. Catal. B: Environ.* **2018**, 227, 114; b) Y. S. Ni, R. Wang, W. T. Zhang, S. Shi, W. X. Zhu, M. S. Liu, C. Y. Yang, X. H. Xie, J. L. Wang, *Chem. Eng. J.* **2021**, 404, 126528; c) P. F. Xia, S. W. Cao, B. C. Zhu, M. J. Liu, M. S. Shi, J. G. Yu, Y. F. Zhang, *Angew. Chem., Int. Ed.* **2020**, 59, 5218.
- [13] F. Li, Z. X. Yu, H. Shi, Q. B. Yang, Q. Chen, Y. Pan, G. Y. Zeng, L. Yan, *Chem. Eng. J.* **2017**, 322, 33.
- [14] Y. N. Liu, Y. L. Su, J. Y. Guan, J. L. Cao, R. N. Zhang, M. R. He, K. Gao, L. J. Zhou, Z. Y. Jiang, *Adv. Funct. Mater.* **2018**, 28, 1706545.
- [15] Y. H. Cai, D. Y. Chen, N. J. Li, Q. F. Xu, H. Li, J. H. He, J. M. Lu, *Adv. Mater.* **2020**, 26, 2001265.
- [16] Y. Wang, B. Y. Gao, Q. Y. Yue, Z. N. Wang, *J. Mater. Chem. A* **2020**, 8, 19133.
- [17] Y. H. Shi, J. H. Huang, G. M. Zeng, W. J. Cheng, J. L. Hu, *J. Membr. Sci.* **2019**, 584, 364.
- [18] W. Barthlott, M. Mail, B. Bhushan, K. Koch, *Nano-Micro Lett.* **2017**, 9, 23.
- [19] Y. Y. Liu, X. L. Guo, Z. T. Chen, W. J. Zhang, Y. X. Wang, Y. M. Zheng, X. Tang, M. Zhang, Z. B. Peng, R. Li, Y. Huang, *Appl. Catal. B: Environ.* **2020**, 266, 118624.
- [20] a) N. Li, Y. Tian, J. H. Zhao, J. Zhang, W. Zuo, L. C. Kong, H. Cui, *Chem. Eng. J.* **2018**, 352, 412; b) I. Papailias, N. Todorova, T. Giannakopoulou, N. Ioannidis, P. Dallas, D. Dimotikali, C. Trapalis, *Appl. Catal. B: Environ.* **2020**, 268, 118733.
- [21] a) Y. H. Guo, F. Zhao, X. Y. Zhou, Z. C. Chen, G. H. Yu, *Nano Lett.* **2019**, 19, 2530; b) F. Yang, J. X. Chen, Z. Y. Ye, D. W. Ding, N. V. Myung, Y. D. Yin, *Adv. Funct. Mater.* **2020**, 2006294.
- [22] W. J. Kong, Y. Gao, Q. Y. Yue, Q. Li, B. Y. Gao, Y. Kong, X. D. Wang, P. Zhang, Y. Wang, *J. Hazard. Mater.* **2020**, 388, 121780.
- [23] C. K. Yao, A. L. Yuan, Z. S. Wang, H. Lei, L. Zhang, L. M. Guo, X. P. Dong, *J. Mater. Chem. A* **2019**, 7, 13071.
- [24] M. J. Liu, S. T. Wang, L. Jiang, *Nat. Rev. Mater.* **2017**, 2, 17036.
- [25] M. Q. Hovish, F. Hilt, N. Rolston, Q. Xiao, R. H. Dauskardt, *Adv. Funct. Mater.* **2019**, 29, 1806421.
- [26] J. C. Zhang, L. F. Liu, Y. Si, J. Y. Yu, B. Ding, *Adv. Funct. Mater.* **2020**, 30, 2002192.
- [27] X. Y. Chen, D. Y. Chen, N. J. Li, Q. F. Xu, H. Li, J. H. He, J. M. Lu, *ACS Appl. Mater. Interfaces* **2019**, 11, 23789.
- [28] a) L. Y. Zhang, Y. He, P. Y. Luo, L. Ma, Y. Fan, S. H. Zhang, H. Shi, S. S. Li, Y. L. Nie, *J. Mater. Chem. A* **2020**, 8, 4483; b) Z. J. Wang, G. J. Liu, S. S. Huang, *Angew. Chem., Int. Ed.* **2016**, 128, 14830.
- [29] X. Q. Cheng, Z. K. Sun, X. B. Yang, Z. X. Li, Y. J. Zhang, P. Wang, H. Liang, J. Ma, L. Shao, *J. Mater. Chem. A* **2020**, 8, 16933.
- [30] H. R. Zhang, A. U. Mane, X. B. Yang, Z. J. Xia, E. F. Barry, J. Q. Luo, Y. H. Wan, J. W. Elam, S. B. Darling, *Adv. Funct. Mater.* **2020**, 30, 2002847.
- [31] a) J. R. Wu, W. W. Wang, Y. Tian, C. X. Song, H. Qiu, H. Xue, *Nano Energy* **2020**, 77, 105122; b) H. P. Mota, R. F. N. Quadrado, B. A. Iglesias, A. R. Fajardo, *Appl. Catal. B: Environ.* **2020**, 277, 119208; c) Y. X. Wang, H. Wang, F. Y. Chen, F. Cao, X. H. Zhao, S. G. Meng, Y. J. Cui, *Appl. Catal. B: Environ.* **2017**, 206, 417.
- [32] C. Lops, A. Ancona, K. D. Cesare, B. Dumontel, N. Garino, G. Canavese, S. Hernandez, V. Cauda, *Appl. Catal. B: Environ.* **2019**, 243, 629.
- [33] W. Z. Yin, W. Z. Wang, L. Zhou, S. M. Sun, L. Zhang, *J. Hazard. Mater.* **2010**, 173, 194.
- [34] C. Worathitanon, K. Jangyubol, P. Ruengrungrong, W. Donphai, W. Klysubun, N. Chanlek, P. Prasitchoke, M. Chareonpanich, *Appl. Catal. B: Environ.* **2019**, 241, 359.
- [35] W. J. Ong, L. L. Tan, Y. H. Ng, S. T. Yong, S. P. Chai, *Chem. Rev.* **2016**, 116, 7159.
- [36] a) S. Zhang, P. C. Gu, R. Ma, C. T. Luo, T. Wen, G. X. Zhao, W. C. Cheng, X. K. Wang, *Catal. Today* **2019**, 335, 65; b) L. C. Chen, J. B. Song, *Adv. Funct. Mater.* **2017**, 27, 1702695.
- [37] P. Yadava, S. T. Nishanthi, B. Purohit, A. Shanavas, K. Kailasam, *Carbon* **2019**, 152, 587.
- [38] a) N. Tian, H. W. Huang, X. Du, F. Dong, Y. H. Zhang, *J. Mater. Chem. A* **2019**, 7, 11584; b) H. X. Zhao, H. T. Yu, X. Quan, S. Chen, Y. B. Zhang, H. M. Zhao, H. Wang, *Appl. Catal. B: Environ.* **2014**, 46, 152.
- [39] R. Li, Y. L. Ren, P. X. Zhao, J. Wang, J. D. Liu, Y. T. Zhang, *J. Hazard. Mater.* **2019**, 365, 606.